

Joint Microseismic Event Detection and Location with a Detection Transformer

Yuanyuan Yang¹, Claire Birnie¹, and Tariq Alkhalifah¹

¹Physical Science and Engineering Division, King Abdullah University of Science and Technology

Key Points:

- A machine learning based procedure is proposed for detecting and locating microseismic events jointly in real time.
- A network architecture combining a CNN and an encoder-decoder Transformer is utilized to extract event information in seismic recordings.
- A set-based Hungarian loss function is applied to handle multiple events within one seismic recording segment.

arXiv:2307.09207v1 [physics.geo-ph] 16 Jul 2023

Corresponding author: Yuanyuan Yang, yuanyuan.yang@kaust.edu.sa

Abstract

Microseismic event detection and location are two primary components in microseismic monitoring, which offers us invaluable insights into the subsurface during reservoir stimulation and evolution. Conventional approaches for event detection and location often suffer from manual intervention and/or heavy computation, while current machine learning-assisted approaches typically address detection and location separately; such limitations hinder the potential for real-time microseismic monitoring. We propose an approach to unify event detection and source location into a single framework by adapting a Convolutional Neural Network backbone and an encoder-decoder Transformer with a set-based Hungarian loss, which is applied directly to recorded waveforms. The proposed network is trained on synthetic data simulating multiple microseismic events corresponding to random source locations in the area of suspected microseismic activities. A synthetic test on a 2D profile of the SEAM Time Lapse model illustrates the capability of the proposed method in detecting the events properly and locating them in the subsurface accurately; while, a field test using the Arkoma Basin data further proves its practicability, efficiency, and its potential in paving the way for real-time monitoring of microseismic events.

Plain Language Summary

During the processes of reservoir stimulation, fluids are injected into a specific area underground. The high-pressure condition created by the fluid injection causes rocks to crack to release the built-up stress, resulting in small earthquakes called microseismic events. Detecting these events in seismic recordings and locating them back to their subsurface locations are important for understanding the subsurface conditions such as fracture networks and fluid flow pathways. This knowledge is critical for applications like carbon storage, geothermal energy extraction, and oil/gas production. Traditional approaches for microseismic event detection and location often suffer from manual intervention and/or heavy computation, while current machine learning-assisted approaches typically address detection and location separately. These limitations prevent the potential for real-time microseismic monitoring, which is crucial for scientists and engineers to make instant, informed decisions, like optimization of injection strategies. Here, we proposed a machine learning-based procedure for simultaneously detecting and locating microseismic events within a single framework, using a conventional Convolutional Neural Network and an encoder-decoder Transformer. Tests on synthetically-generated and field-collected passive seismic data illustrate the accuracy, efficiency, and potential of the proposed method, which could pave the way for real-time monitoring of microseismic events in the future.

1 Introduction

From its inception in the 1970s and its later practical usage around 2000, microseismic monitoring has been helping us understand subsurface changes over time and processes that cause them (Warpinski, 2009). While its most common use to date has been hydraulically-induced fracture mapping (Shapiro et al., 2006), it is also used for reservoir surveillance, CO_2 sequestration monitoring, seismic hazard assessment, and many other applications in the energy and mining industries (Maxwell et al., 2010; Kaven et al., 2015; Perol et al., 2018). Among the information extracted from microseismic monitoring, the detection of microseismic events from the long seismic recordings and the estimation of their corresponding source locations are two primary components for observing, diagnosing, and acting upon the dynamic indications in the reservoir evolution and health. By tracking the fracturing properly, invaluable insights into the subsurface are gathered to optimize our strategies in, for example, enhanced geothermal systems (EGS) or carbon capture, utilization, and storage (CCUS) projects, and also to mitigate the environmental risks arising from induced seismicity (Young & Maxwell, 1992; Folesky et al., 2016; Li et al., 2022). These important objectives call for exhaustive solutions to microseismic event detection and location.

Conventionally, microseismic event detection and location are typically addressed separately as two streams of tasks, and their corresponding methods are designed to be highly accurate or generic. However, for the majority of cases, such advantages come at a price, either requiring extensive human expertise or large computational overhead. For microseismic event detection, the short-term average to long-term average (STA/LTA) method (Allen, 1978), as one of the most widely used techniques for full-field detection, and most of its adaptations depend upon careful selection of parameters (such as window size and threshold) to reflect actual signal and noise conditions and complicated re-adjustment when the recording condition changes (Vaezi & Van der Baan, 2015; Kumar et al., 2018; Zheng et al., 2018). Alternative detection methods like waveform template matching (Gibbons & Ringdal, 2006) have proven to be computationally intensive and time-consuming (Skoumal et al., 2016). For microseismic event location, traveltime-based methods (Waldhauser & Ellsworth, 2000; Eisner et al., 2009) require manual labor in traveltime picking, and thus suffer from the heavy workload of human interaction and suffer from manual picking errors (Bose et al., 2009), while migration-based (McMechan, 1982; Larmat et al., 2006) and inversion-based location methods (Sun et al., 2016; Wang & Alkhalifah, 2018; Song et al., 2019) demand large computational memory and time for simulating the wavefields. The common requisite nowadays is to detect and locate the majority of microseismic events in a short time (i.e., real-time) in order to make instantly-informed decisions. Therefore, there is still a practicability gap towards the real-time field implementation of these methods.

Machine learning (ML) driven approaches can overcome the substantial limitations of manual intervention and/or high computational cost from conventional approaches and promise the possibility for real-time results in detecting and locating microseismic events, once the model is trained properly. In contrast to conventional approaches, ML-driven approaches effectively front-load the computational burden to the offline time (i.e., the training stage), whereas online (i.e., the inference stage), the trained models can fulfill the evaluations on the order of seconds (Grady et al., 2022). These approaches are therefore attractive for applications that require a large number of executions/iterations and demand real-time completion, since data generation and model training are covered at the offline stage. Much work has been in utilizing ML in microseismic monitoring (Anikiev et al., 2023). ML-driven methods for microseismic event detection can be divided based on what is the input to ML algorithms, for example either a single trace or full arrays. Trace-based methods (e.g., Zheng et al., 2018; Chen, 2020; Wilkins et al., 2020) take the input as a sequence. For example, Birnie and Hansteen (2022) introduced a bidirectional recurrent neural network for accurate event detection via taking this task as binary classification for trace-wise recordings. The pitfall of such trace-based methods is that the arrays are not fully utilized, especially considering the poor signal-to-noise ratio (SNR) of microseismic data. On the contrary, array-based methods (e.g., Horne et al., 2019; Birnie et al., 2021; Shaheen et al., 2021) treat the input as an image and thus can take advantage of array information like moveout patterns of energy across the sensors. Stork et al. (2020) provided one of the earliest successful examples, in which they trained the convolutional neural network (CNN) known as YOLOv3 to detect events based on the waveforms in array recordings. ML-driven methods for microseismic event location, similar to traditional location techniques, are mostly based on dense arrays of receivers. This is because microseismic data have less favorable SNR and are more sensitive to local heterogeneities compared to global seismology, which requires more information and features to locate the events. ML methods for event location utilize either the arrival times (Huang et al., 2018) or the full waveforms (Wamriew et al., 2020; Wang et al., 2021) to map the events to subsurface locations. There is also another interesting branch of research which uses the so-called physics-informed neural networks (PINNs) to locate microseismic events (Grubas et al., 2021; Izzatullah et al., 2022; Huang & Alkhalifah, 2023). These approaches, with very fast runtime during inference, are friendly to practical situations that require instant processing.

Nevertheless, the separation of event detection and location as individual tasks still discourages the real-time adaptation of the aforementioned methods. To simultaneously detect

and locate events within the seismogram segment, Wang and Alkhalifah (2021) designed two CNNs: one of which aims to predict the number of events and the other is responsible for locating the present events. This method offers the opportunity of real-time computation when detecting and locating events. However, given that these two tasks are utilizing the same information (i.e., the waveforms), we believe it would be more beneficial to have a joint microseismic event detection and source location network that takes us from the recorded waveforms directly to the locations of the events responsible for these waveforms.

In this work, we unify microseismic event detection and location into a single framework by adapting the original DETection TRansformer (Carion et al., 2020), which is based on a CNN backbone and a Transformer encoder-decoder general architecture with a set-based Hungarian loss. Using synthetic data from a 2D profile of the SEAM Time Lapse model and field data from the Arkoma Basin in North America, we demonstrate the robustness, efficiency, and transformative potential of the proposed approach for concurrent detection and location of microseismic events in real-time applications. The contributions of this work can be summarized as follows: (1) a pioneering introduction of an ML-based framework for microseismic event detection and location, trained offline on synthetic data; (2) leveraging the DETection TRansformer network and a Hungarian loss to address the challenge of handling multiple events within a given recording segment; (3) conceptual proof and practical validation of the proposed method through successful applications on synthetic and field passive seismic recordings.

The subsequent sections of this paper are organized as follows: we start by describing essential elements of our approach, including the DETection TRansformer model, its inputs and outputs, as well as the loss function computation; following this, we present the results on synthetic passive seismic data to assess the approach accuracy; a field data application highlights the advantages and limitations of the approach, which will be further discussed in detail in the Discussion section; we conclude this study at the end.

2 Methods

Several ingredients are essential for joint microseismic event detection and location within a unified framework: (1) a network architecture that simultaneously predicts the number of events (a classification task) and the corresponding source locations of existing events (a regression task); (2) a series of data processing procedures to remove the need of source ignition time and to mitigate the discrepancies between synthetic (training) and field (inference) data; (3) a bipartite matching algorithm that ensures unique matching between ground-truth and predicted events for cases where there are multiple events within one input data segment; and (4) a set prediction loss function that utilizes the bipartite matching result and evaluates both detection and location predictions concurrently.

2.1 The DETection TRansformer model

DEtection TRansformer (DETR) is a recently developed framework for object detection, which is a fundamental computer vision task aiming to detect object instances and locate them in images and/or videos. DETR has gained considerable attention due to its contribution towards eliminating the need for many hand-designed components while also demonstrating good performance (Dai et al., 2021; Liu et al., 2022; Zhang et al., 2022). Compared to classical CNN-based object detectors, DETR greatly simplifies the detection pipeline by exploiting the versatile and powerful relation-modeling capabilities of transformers to replace hand-crafted rules including prior knowledge injection, like anchor generation, and post-processing, like non-maximum suppression (Zhu et al., 2020; Wang et al., 2021; Li et al., 2022). The DETR architecture is powerful but conceptually simple; the following briefly describes the general framework, whilst we refer the readers to Carion et al. (2020) for a more in-depth discussion on the original DETR framework.

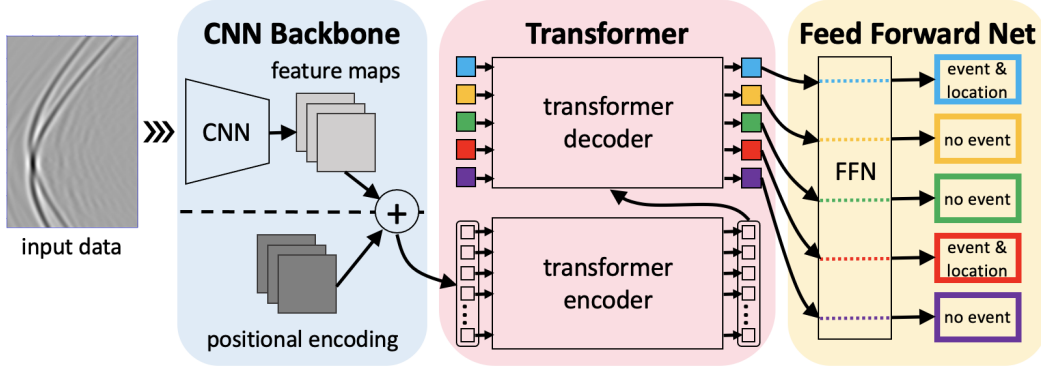


Figure 1. The architecture of DETection TRansformer.

As depicted in Figure 1, DETR contains three main components: a conventional CNN backbone, an encoder-decoder transformer, and a simple feed forward network (FFN). Fed with an input passive seismic data segment, the CNN backbone generates a high-level activation map for extracting a compact feature representation. Considering the following transformer architecture is permutation-invariant, DETR also supplements the feature maps with positional encodings to inject position information into the feature space.

Given the feature maps extracted from the CNN backbone, DETR leverages a standard transformer encoder-decoder architecture to transform the input feature maps into features of a set of prediction sequences using a multi-headed attention mechanism. The encoder expects sequences as inputs, therefore each two-dimensional feature map is flattened in the spatial dimension into a one-dimensional feature vector. For the decoder, the inputs include both output feature vectors from the encoder and N input embeddings, where N should be set to a value significantly larger than the typical number of expected events within one input passive seismic data segment. These input embeddings, which are denoted by the colorful boxes fed to the transformer decoder in Figure 1, are learnable positional encodings that are referred to as object queries. There are two types of attention modules in the decoder: cross-attention and self-attention modules. In the cross-attention module, object queries extract features from the feature vectors. In the self-attention module, object queries interact with each other to capture their own relationships (e.g., to prevent predicting duplicated events). To conclude, the transformer component infers a fixed-size set of N predictions in a single pass through the decoder. In this work, we assume the maximum number of events, for test purposes, in the input windowed seismic segment is three, and thus, we set N to five in its application.

The N prediction sequences produced by the decoder are then passed to the FFN and independently decoded to make N final predictions. There are two branches inside the FFN. One branch acts as a classification branch to produce the probabilities of an event existing within a prediction slot using a softmax activation function. Once the probability is larger than a determined threshold (e.g., 0.7 chosen in this work - as it was in the original DETR paper), an event is assumed to be detected in this slot. The other branch functions as a regression branch to predict the corresponding source coordinate locations within the area of interest in the subsurface model.

2.2 Network inputs: data processing

In this application, the input data to the DETR network are passive seismic recordings. To train the network, synthetic passive seismic data are first modeled with seismic events generated from potential source locations using a velocity model that best represents

the subsurface area of interest (e.g., a tomography inversion model). Due to the fact that microseismic events are generally weak in terms of energy and magnitude, for subsurface monitoring applications only transmission P-wave components are typically used. Accordingly, we resort to the acoustic assumption and consider the locations of microseismic events as point sources. The acoustic wave equation offers a more efficient alternative, than a more realistic elastic wave equation, to generate the larger volume of passive seismic data containing microseismic events randomly ignited in the region of interest, which is needed for training the network. The suggested approach can be easily adaptable to an elastic or an anisotropic assumption of the Earth, which simply involves using the corresponding wave equation for modeling the training samples. However, it also requires knowledge of the corresponding medium parameters, like the shear wave velocity, or the elastic coefficients of the investigated area.

To help adapt the training on synthetic data to field data application, instead of directly using the lengthy seismic recordings as inputs to the network, the recordings are sliced into relatively short segments and processed using the MLReal domain adaptation technique (Alkhalifah et al., 2022), which involves a series of efficient linear operations including cross-correlation, auto-correlation, and convolution between the synthetic and field data. These operations transform the features of the training dataset (i.e., the synthetic data) to incorporate those of the application dataset (i.e., the field data), and vice versa, bringing their distributions much closer to each other. This can improve the generalization of the synthetically-trained ML models on field data.

The new training data, $D_{train}(x, \tau)$, which is the synthetic passive seismic data transformed by the MLReal technique, can be defined as follows:

$$D_{train}(x, \tau) = [d_{syn}(x, t) \otimes d_{syn}(x = x_{ref}, t)] * [d_{fld}(x, t) \otimes d_{fld}(x, t)], \quad (1)$$

where $d_{syn}(x, t)$ is the synthetic seismic data segment, $d_{fld}(x, t)$ is a random sample of the field data segment, x_{ref} is a fixed-location reference trace, \otimes symbolizes the cross- or auto-correlation operation and $*$ represents the convolution operation. Specifically, the correlation and convolution operations convert the second axis from the time dimension t to the lag dimension τ . In other words, Equation 1 represents the cross-correlation of the synthetic data segment with a fixed reference trace extracted from the segment itself and then the convolution of the resulting data with a random sample of the auto-correlated field data segment.

As for the new testing/application data, $D_{test}(x, \tau)$, the MLReal transformation is given by:

$$D_{test}(x, \tau) = [d_{fld}(x, t) \otimes d_{fld}(x = x_{ref}, t)] * \left[\frac{1}{n} \sum_{j=1}^n d_{syn}^j(x, t) \otimes d_{syn}^j(x, t) \right], \quad (2)$$

where n is the total number of synthetic data segments in the training set. It includes the same operations as in Equation 1 with the role of synthetic and field data reversed. Furthermore, the mean of the auto-correlated synthetic data segments is utilized instead of a random sample. The above MLReal domain adaptation technique helps to bridge the gap between training on synthetic data and applications on field data by incorporating realistic features into the synthetic training data. Figure 2 shows the MLReal transformation for both the training and application data. Note how similar the data features are after this domain adaptation. If the generated synthetic data are realistic enough, in which domain adaptation is not needed, the second part of Equations 1 and 2 (the auto-correlation) can be removed, which leaves us with the cross-correlation part as in Wang et al. (2021).

The correlation operation has moved all the existing events within a long recording segment to the zero-lag area, regardless of their original arrival time. Therefore, in practice, segmentation of a fixed area around the zero lag and resampling can be applied to

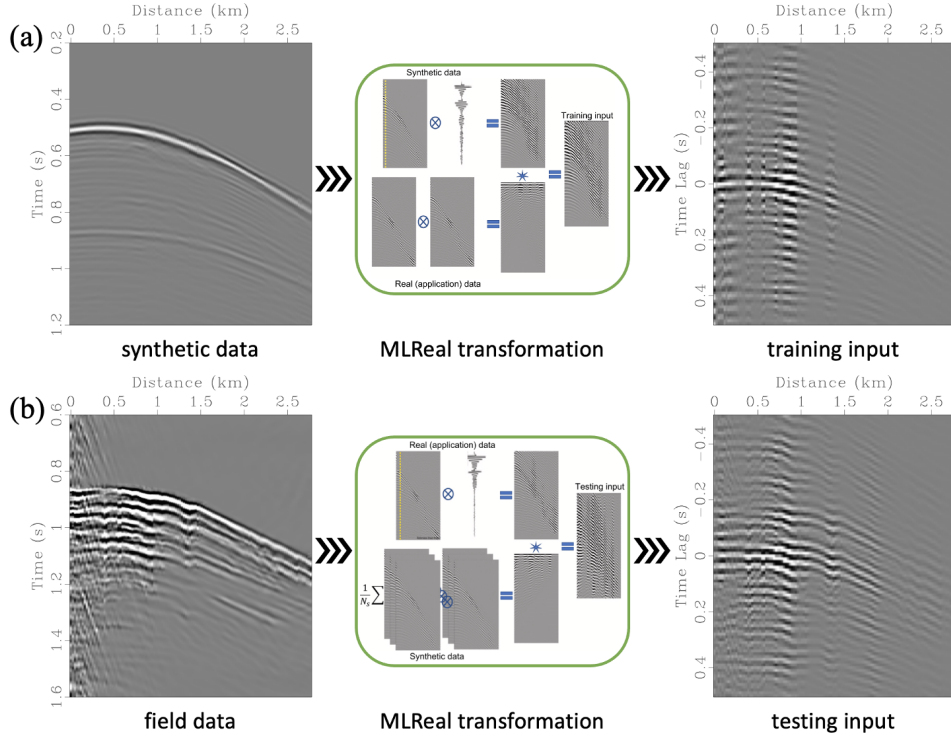


Figure 2. The MLReal transformation diagram for (a) training data and (b) application data, respectively.

significantly reduce the input data size without losing useful event information (e.g., their curvature). In the interest of reducing the cost of generating synthetic data with varying numbers of events, we prepare the multiple-event synthetic training data by combining (stacking) modeled single-event data. This allows fast generation of a significant volume of training samples without the need for costly modeling of each multi-event scenario. This could be considered as a form of data augmentation.

2.3 Network outputs: bipartite matching

One of the main difficulties of training is to score predicted outputs (probabilities of event existence and corresponding source locations) with respect to the ground truth, particularly when dealing with an unknown number of microseismic events within recorded segments. As previously mentioned, DETR infers a fixed number of N predictions, where N is usually much larger than the expected maximum number of events in one input windowed seismic segment. Therefore, to be consistent with the size of predictions, the ground truth in this application is padded to a set of size N using a special “no event” label, which represents an absence of an event within a slot.

To successfully address the challenge of multiple events in one input segment, it is crucial to consider the ordering of labels with respect to the individual events. Wang and Alkhalifah (2021) chose to concatenate the locations of multiple events in a predefined order (a.k.a., they ordered the events based on the arrival time) as a target sequence during training. However, the source locations of existing events are inherently an unordered set rather than an ordered sequence. Imposing a predefined order usually gives rise to the following intractable problems. First, it introduces bias in the training stage, which can highly penalize shifts in the order between locations (Ye et al., 2021). In other words, even

if the network makes accurate predictions for each event, a shift in the ordering still results in a large training loss. Second, the predefined order increases the difficulty of training the network since the network needs to learn this special pattern that we have created.

In real-world scenarios, windowed seismic recording segments may contain zero, one, or several microseismic events. The actual number of events within one particular segment is often unknown, and perhaps more importantly, this number varies from one segment to another. To deal with this, the outputs of this application should be naturally expressed as sets of entities rather than vectors or sequences. In contrast to a vector or sequence, a set is a collection of elements which is invariant under permutation of the order of elements, and its size is not fixed in advance (Rezatofghi et al., 2017). A pioneering solution for predicting a set is to find a bipartite matching between the ground truth and predictions based on the Hungarian algorithm, which is a widely used algorithm in graph matching. Given a cost matrix, the algorithm provides an optimal matching result (Li et al., 2022). A loss function based on this remains invariant to changes in the ordering of predictions.

Let us denote $y = \{y_i\}_{i=1}^N$ as the ground-truth set of events after padding, and $\hat{y} = \{\hat{y}_i\}_{i=1}^N$ as the set of N predictions. To find a bipartite matching between these two sets, we search for a permutation of N elements $\sigma \in \mathfrak{S}_N$ with the lowest cost:

$$\sigma^* = \arg \min_{\sigma \in \mathfrak{S}_N} \sum_{i=1}^N \mathcal{L}_{\text{match}} \left(y_i, \hat{y}_{\sigma(i)} \right), \quad (3)$$

where $\mathcal{L}_{\text{match}} \left(y_i, \hat{y}_{\sigma(i)} \right)$ is a pair-wise matching cost between the ground truth y_i and a prediction with index $\sigma(i)$. This optimal assignment can be completed efficiently through the Hungarian algorithm.

The matching cost takes into consideration both the classification accuracy and location error. Each element i of the ground truth set can be seen as $y_i = (c_i, s_i)$, where c_i is 1 when an event is present in this slot and 0 for the “no event” case (i.e., a binary classification task), and $s_i \in [0, 1]^2$ is a vector that defines the normalized source coordinate locations in reality, relative to the region of interest in a two-dimensional case. For the prediction with index $\sigma(i)$, we define the probability of class c_i as $\hat{p}_{\sigma(i)}(c_i)$ and the predicted source location as $\hat{s}_{\sigma(i)}$. With these notations, we define

$$\mathcal{L}_{\text{match}} \left(y_i, \hat{y}_{\sigma(i)} \right) = \left\| c_i - \hat{p}_{\sigma(i)}(c_i = 1) \right\| + \mathbb{1}_{\{c_i \neq 0\}} \mathcal{L}_{\text{MSE}} \left(s_i, \hat{s}_{\sigma(i)} \right), \quad (4)$$

where $\|\cdot\|$ computes the absolute value of the element inside it, $\mathcal{L}_{\text{MSE}}(\cdot)$ is the mean squared error (MSE) loss function, $\mathbb{1}_{\{c_i \neq 0\}}$ represents the indication function which equals 1 when an event is actually present in the i^{th} slot and equals 0 otherwise.

2.4 Network training: the Hungarian loss

The next step after the bipartite matching is to compute the so-called Hungarian loss for all pairs matched in the previous step. The loss can be defined as a linear combination of the binary cross-entropy (BCE) loss for class predictions and the mean squared error loss for location predictions:

$$\mathcal{L}_{\text{Hungarian}}(y, \hat{y}) = \sum_{i=1}^N \left[\mathcal{L}_{\text{BCE}} \left(c_i, \hat{p}_{\sigma^*(i)}(c_i) \right) + \mathbb{1}_{\{c_i \neq 0\}} \mathcal{L}_{\text{MSE}} \left(s_i, \hat{s}_{\sigma^*(i)} \right) \right], \quad (5)$$

where σ^* is the optimal assignment computed in Equation 3. The use of the BCE loss is different from what we use in the matching cost, since the absolute difference between ground-truth and predicted probabilities offers a faster computation of the cost matrix. During the implementation, the classification loss term is down-weighted to compensate the data and class imbalance by applying a 1:9 ratio between the classification and location loss terms.

3 Numerical Examples

The proposed approach is first validated on synthetic passive seismic data as a conceptual proof, where we analyze the accuracy with respect to multi-event detection and location. Afterwards, we apply this approach to a real-world microseismic dataset obtained from the field for a practical attestation of it.

3.1 The SEAM Time Lapse model example

The SEAM Time Lapse model is chosen to imitate a scenario of CO_2 injection and microseismic event induction to test our proposed approach. To mimic real conditions, as mentioned above, the training and validation data are generated using a smooth subsurface model, as if it was obtained from migration velocity analysis, while the test (assumed real) data are generated using the true subsurface model. In total, 500 zero-event, 2000 one-event, 2000 two-event, and 2000 three-event seismic segment samples are generated to train the network. Detecting if there is any event or not is a relatively simple task for the network. Thus, substantially less zero-event training data are needed for the training. An additional benefit of this is that it helps to reduce the training cost. Each sample is made up of the preprocessed seismic data, labels of the number of events, and labels of their corresponding source coordinate locations. White Gaussian noise is added to the training and validation data in between training iterations to mimic real-life scenarios where perfectly clean data are unavailable. The noise injection can also improve the network performance by allowing some inaccuracy when training networks (Luo & Yang, 2014). During the inference stage, the same level of noise is also incorporated in the test data.

The trained network demonstrates its competence in detecting microseismic events within the input seismic segments. Testing it on 1000 test samples from each class (i.e., zero-, one-, two-, and three-event cases, respectively), the classification accuracy is assessed via a confusion matrix as shown in Table 1. Remarkably, the network achieves a flawless accuracy of 100% for the simple task of event presence detection. Furthermore, the network robustly performs above 90% accuracy in classifying the number of events within one input segment across all cases. These results highlight the strong capability of this approach in accurately detecting microseismic events in the input seismic segment. Notably, the slightly lower classification accuracy observed in the one-event case is due to the fact that the two-event and three-event inputs may be occasionally interpreted as a single event by the network if the events' sources are closely located.

Table 1 Classification Results (Unit: %)

		Predicted			
		0-event	1-event	2-event	3-event
Actual	0-event	100	0	0	0
	1-event	0	91.8	8.2	0
	2-event	0	0	93.5	6.5
	3-event	0	0	1.6	98.4

The accuracy of locating microseismic events back to their subsurface sources is assessed by computing the location errors, which quantify the absolute difference between the predicted and ground-truth source locations of the test data with correct classification predictions. Figures 3(a)-(c) visually depict the maps of the sources located for the one-, two-, and three-event cases, respectively, with the colormap representing the location error values. Figures 3(d)-(f) present the corresponding location error maps after applying Kriging interpolation and Gaussian smoothing, to better illustrate the distribution of errors across the entire domain of interest. Additionally, the average location errors for one-, two-, and three-event cases are 18.4, 25.6, and 39.8 meters, respectively. As expected, the location errors increase as the number of events within the input segment grows, since the network

is dealing with more complicated inputs where events may overlap or interfere with each other. It is worth noting that the area in which we placed the sources for generating the training data is of 1.4 by 0.8 kilometers. Therefore, the average location errors are generally less than 5% with respect to the size of the monitoring region. These results exhibit the capability and reliability of this approach to accurately locate the microseismic events.

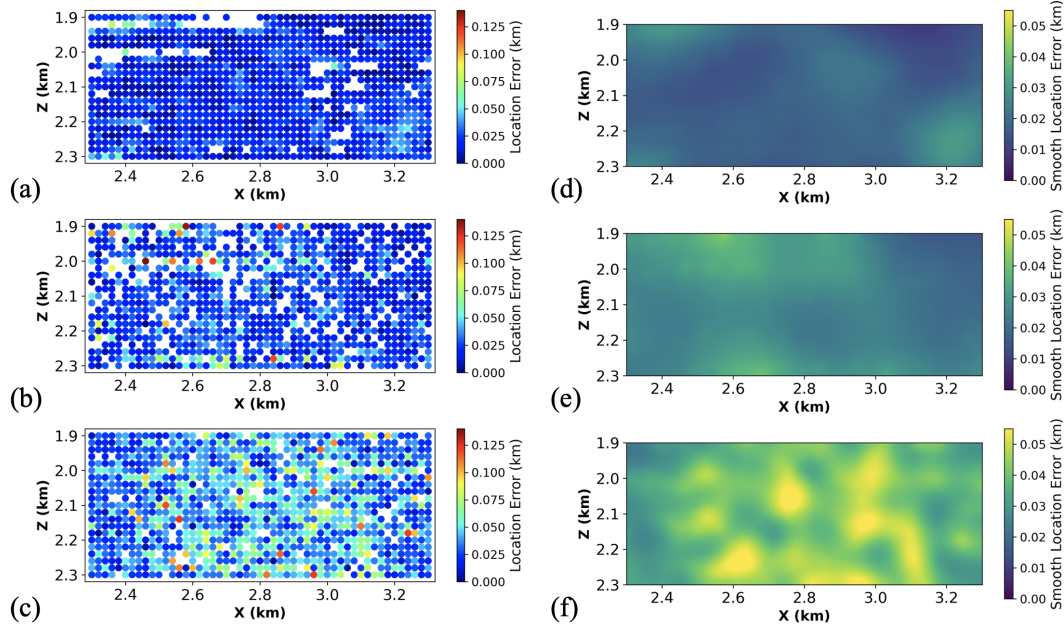


Figure 3. Source location maps of the test data with right classification predictions, colored with the actual location error values, for (a) one-, (b) two-, and (c) three-event cases, and the corresponding location error maps (after Kriging interpolation and Gaussian smoothing) for (d) one-, (e) two-, and (f) three-event cases.

To further explore the sensitivity of source location prediction to the distance between events within a single segment, we perform the following experiment. Over the whole region of potential source location defined earlier, a single source is placed on a regular grid with an interval of 20 meters across both axes to generate 1071 single-event data. Then, the single-event data for each source are added to the data from a source in the center of the domain to generate 1070 double-event data. By inputting these data to the network, location error maps are obtained for the double-event case. Figure 4(a) displays the location errors for the various sources on the regular grid, while Figure 4(b) shows the location errors of a single point, specifically the central source, placed at the location of the grid point in which the other source is located. The white region in the maps represents grid points with wrong one-event classification, indicating inputs where the network failed to distinguish the two events. Clearly, the distance between events significantly influences the location accuracy. The general trend observed is that closer proximity between events leads to lower location accuracy for both events, with the deeper event generally exhibiting better accuracy compared to the shallower one. Moreover, the sensitivity differs in the x- and z-axis directions. The location accuracy is more sensitive to the x-distance. This makes sense since, based on the frequency range (5-20 Hz) and the offset (4.2 kilometers) under consideration, the data exhibit more significant differences when perturbing the event in the x-direction compared to the depth direction. This suggests that horizontal movement of events, which changes the location of its apex, is more significant than variations in

curvature for the neural network. This feature, of course, depends on the frequency band and the aperture of recording.

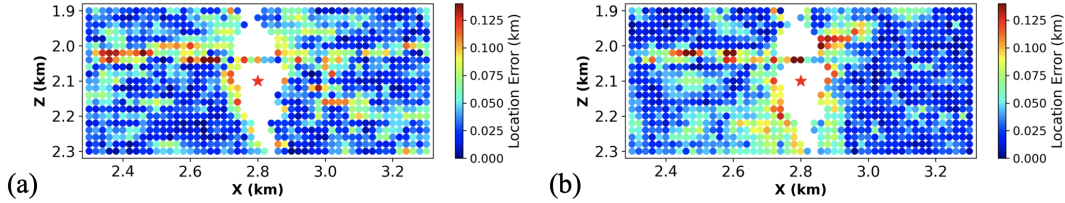


Figure 4. The error maps of source location for (a) sources on the regular grid which are put in their corresponding true locations and (b) the central source placed on the grid point in which the second event is located.

3.2 The Arkoma Basin field data example

The proposed approach is further validated using a passive seismic dataset recorded for the purpose of hydraulic fracture monitoring of a shale gas reservoir in the Arkoma Basin, North America. More information about this dataset can be found in previous work on the same dataset by Staněk and Eisner (2017). Despite being a 3D dataset, we have chosen to initially work with a 2D profile and three previously identified field events on this 2D plane to investigate the applicability of this approach on the field data.

An exploratory data analysis is first conducted on the field data, an example of which is shown in Figure 5(a). To improve the data quality, a simple non-local means method is employed for denoising, as illustrated in Figure 5(b). Across all the field events, it is observed that the right side of the recordings exhibit a moveout pattern substantially more linear in nature than the observed hyperbolic microseismic signals. The calculated propagation velocities for this linear moveout consistently exceed 6500 meters/second. However, the maximum velocity of the subsurface model given by the tomography inversion is 5350 meters/second. This indicates that the linear moveout can be attributed to other subsurface objects rather than the earth itself. Our hypothesis is that these linear moveout events represent head waves that propagated along the horizontal direction within a high-velocity subsurface object, like a tube. Considering that the proposed method is sensitive to the event curvature as indicated in the synthetic sensitivity analysis, the traces corresponding to the linear moveout are removed. The resulting processed field data are presented in Figure 5(c).

To evaluate the efficacy of the proposed approach on the field data, an experiment is carried out for the scenario of single-event detection and location. As such, the training data contain either zero or one event. The network is trained using 2000 synthetic one-event passive seismic segments that are generated based on the provided subsurface model, obtained from a previous active seismic survey (Staněk & Eisner, 2017). The training set also includes an additional 500 zero-event seismic segments. To be consistent with the field data, all the synthetic training data consist of 56 traces spanning the same range as field data. For testing purposes, three field seismic data segments are selected with previously detected and analyzed events (each segment with one event within it), and their reference locations were earlier determined using the velocity model from tomography inversion. By comparing the predicted source locations from the network with the reference locations of these field events, we obtain location errors of 26.0, 60.2, and 48.7 meters, respectively. The inference workflow for one of the field test data is illustrated in Figure 6. These results showcase the impressive performance and accuracy of this approach when applied to real field data for detecting and locating microseismic events from the subsurface.

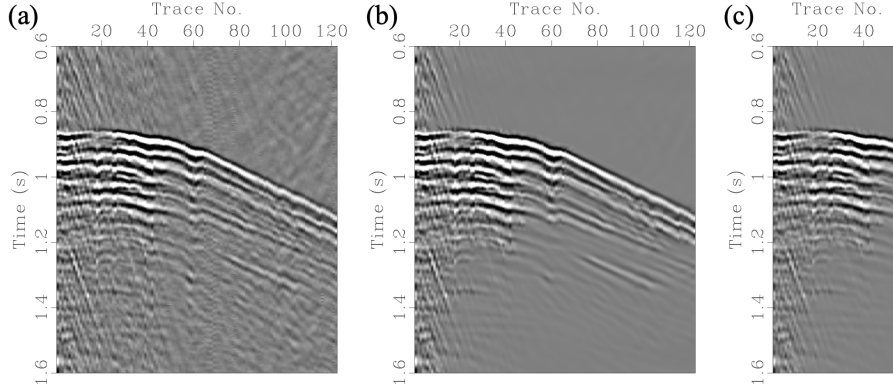


Figure 5. Examples of (a) original field data, (b) denoised field data, and (c) processed field data after removing the traces corresponding to the linear moveout.

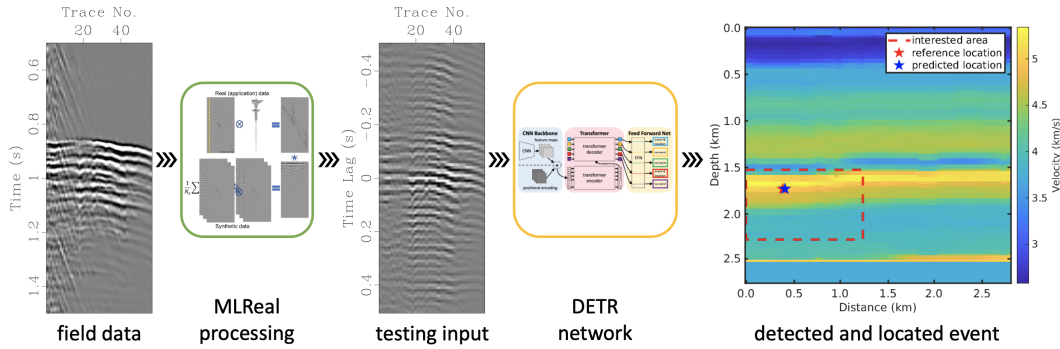


Figure 6. The inference workflow for one of the field test data, where one event is present in it.

The predictions on the three field test data are promising. However, it is crucial to exercise caution as the reference locations utilized are not the absolute ground-truth locations. To obtain a reliable assessment of the actual location accuracy, three synthetic test events are modeled using the reference locations of the field events, and are processed using the MLReal technique to ensure consistency with the training data. The network successfully detects all the three synthetic events with location errors of 145.5, 131.9, and 128.5 meters. Here, further analysis is needed to identify the underlying cause of the location errors in this range.

Two examples of double-event seismic data are simulated, in one of which the two sources are 200 meters away horizontally, while in the other the two sources are 200 meters away vertically, as shown in Figure 7. A red line is used to indicate where we start to cut off the right-hand-side traces corresponding to the linear moveout. The original offset of field data is around 2750 meters. After the trace removal, it is reduced to 1250 meters. Figure 7 demonstrates that: with long offsets like 2500 meters, those two events can still be recognized; however, with short offsets like 1250 meters, it is almost impossible to tell that there are two events. In other words, an inadequate data acquisition will significantly hinder the analysis of the seismic recording. When training and testing the network with the full 122 traces, the location errors from the synthetic test data are around 50 meters, which firmly supports our conclusion.

In this case, two single-event field data are selected and stacked together to simulate a double-event field data, and the workflow of this process is depicted in Figure 8. These two field events are 242 meters away according to their reference locations. However, as

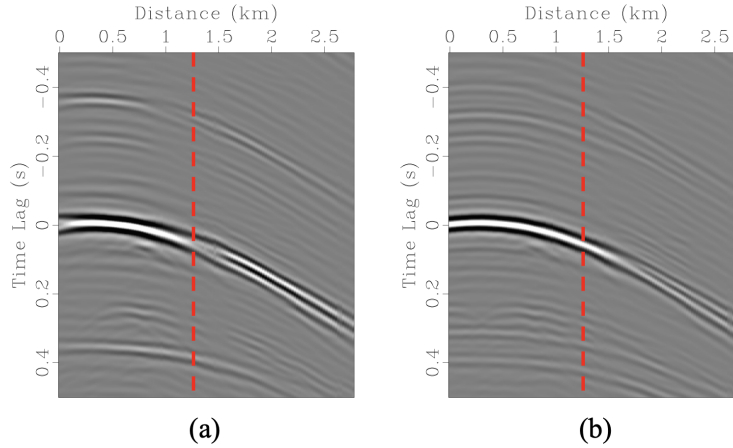


Figure 7. Examples of double-event seismic data where (a) two sources are 200 meters away horizontally, and (b) two sources are 200 meters away vertically. The red dash line lies exactly in where the traces corresponding to the linear moveout are removed.

we can observe, due to the reason stated above, the network is unable to distinguish the two events. This suggests that a reasonable recording aperture is required for any detection and/or location method to be able to distinguish events properly in multi-event segments.

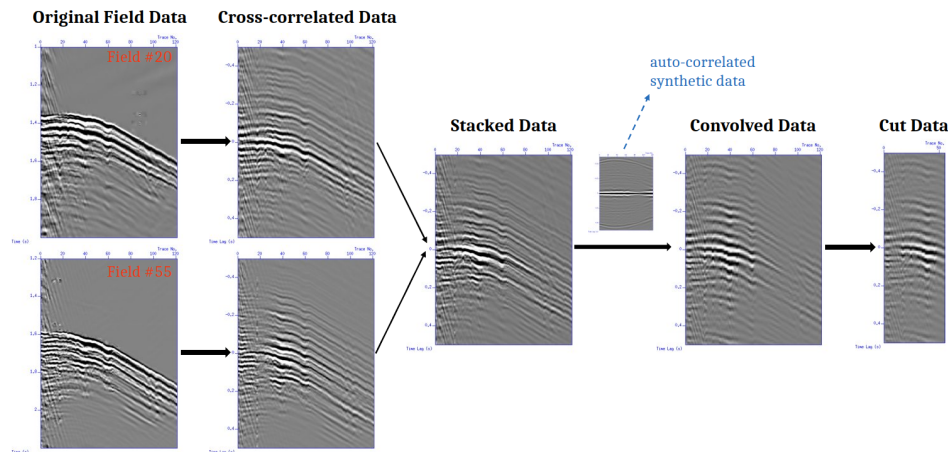


Figure 8. The generation workflow of a double-event test input by stacking two single-event field data.

4 Discussion

4.1 Utilization of MLReal

In this study, we proposed to train the network on synthetic seismic data and apply it to field seismic data. Therefore, the level of similarity between the training and application datasets matters. Often, the synthetic data fail to capture features of the field experiment, like a proper waveform source signature and the ambient noise. Thus, we easily end up with poor performance of trained ML models at the inference stage. This problem in our

application is solved through the MLReal domain adaptation technique, which has also been successfully applied in other work (e.g., Birnie & Alkhalifah, 2022; Zhang et al., 2022). By transforming the distributions of training and application datasets into much closer ones through a series of cross-/auto-correlations and convolutions, MLReal helps the trained models generalize better on field data.

While applying MLReal, the time-axis information is eliminated by the correlation operation. Bringing all the events inside the input segment to the area near zero lag makes the multi-event detection and location harder for cases where events come from very close source locations and therefore exhibit similar moveout patterns. Usually, this might not be an issue for microseismic clustering applications where the shape and extent of the microseismic event cloud is more important than the exact number of events. However, if the number of events is important, one way to deal with this situation is to slice the original recording into shorter segments where the likelihood of each segment containing at most one event is high.

4.2 Real-time monitoring

With our proposed method, the heavy computational burden is charged during the network training stage, which is offline. At the inference stage, all the processing procedures on the field data (including segmentation, cross-correlation, and resampling) are very efficient to apply. More importantly, the inference time of each input data is on the order of 10^{-3} seconds. Thus, once the network is adequately trained, it can be applied for joint microseismic event detection and location with a real-time completion. In addition to this, it can be in service for a long time (e.g., for months) at the cost of one-time training, unless the subsurface velocity model or acquisition geometry is updated. This ensures that engineers and scientists are informed of the locations of events in the field instantly. For incorporating MLReal, we have to utilize some field data in the training, which can be done over a short period of time. Once enough features of the real data are incorporated in the training, the application of the network for real-time monitoring should be possible.

Previously, Wang and Alkhalifah (2021) proposed the use of two separate networks for simultaneously detecting and locating microseismic events. In such cascading systems, the input data and information go from one network to another. However, tasks like event detection and location make use of the same features in the input seismic data, which is the waveform. Mousavi et al. (2020) illustrated that for the scenario of earthquake monitoring, combining these two tightly-related tasks jointly in a single framework improves the model performance in each individual task. Moreover, feeding (almost) the same input data to two different networks and train them separately is generally inefficient. Finally, the application of an end-to-end framework will be faster than two networks in tandem for inference (assuming similar complexity of the network architectures).

4.3 Future work

In this study, we have proven the value of the DETR framework assuming a single receiver line. However, surface microseismic monitoring arrays are typically two-dimensional, resulting in 3D datasets of x, z, t . Incorporating the additional spatial axis is likely to further improve our procedure due to the additional signal information available. For 3D applications, our approach doesn't demand densely and uniformly sampled seismic data. For the extension to 3D, two choices are available: (1) concatenating all the sensor lines in a horizontal distance axis and taking it as a 2D image as the input to the network, which requires no modification to the current network architecture; or (2) taking different 2D lines as different channels to the CNN backbone, as performed by Wang et al. (2021), which is also implementation-wise simple since it only requires a change in the number of input channels in the CNN backbone from one to the number of sensor lines in the survey.

Another extension would be the transformation from an acoustic assumption to an elastic one. This could be easily achieved by changing the velocity model used for generating the synthetic training data. Next, by substituting class loss term from the binary cross-entropy loss to the multi-class cross-entropy loss function, this approach will naturally learn to handle P- and S-wave events within the seismic recordings. Apart from being closer to the real-world situations, more signals with their corresponding features in the seismic segments would hopefully improve the accuracy of the trained network.

5 Conclusions

We proposed an approach adapted from the DETECTION TRANSFORMER for joint microseismic event detection and location directly applied on the recorded seismic waveforms. The proposed network is built on a CNN backbone with a Transformer encoder-decoder block and trained using a set-based Hungarian loss. A synthetic study validated the strong competence of the proposed procedure. Furthermore, the procedure was applied to a field dataset from the Arkoma Basin, which evaluated its practicability and accuracy, and identified the acquisition conditions under which we can obtain optimal performance. Once trained, the network offers an end-to-end solution for real-time monitoring to detect and locate microseismic events. Due to its ability to analyse varying number of microseismic events on-the-fly, we believe this work will pave the way for a new generation of real-time ML algorithms for joint microseismic event detection and characterisation.

Open Research Section

The synthetic datasets in this paper are available at <https://zenodo.org/record/8128526>.

Acknowledgments

This publication is based on work supported by King Abdullah University of Science and Technology (KAUST). The authors thank the DeepWave sponsors for their support and Microseismic Inc. for the use of the Arkoma Basin field data. Appreciation also goes to Xinquan Huang and Hanchen Wang for the useful discussions and suggestions.

References

- Alkhalifah, T., Wang, H., & Ovcharenko, O. (2022). Mlreal: Bridging the gap between training on synthetic data and real data applications in machine learning. *Artificial Intelligence in Geosciences*, 3, 101–114.
- Allen, R. V. (1978). Automatic earthquake recognition and timing from single traces. *Bulletin of the seismological society of America*, 68(5), 1521–1532.
- Anikiev, D., Birnie, C., bin Waheed, U., Alkhalifah, T., Gu, C., Verschuur, D. J., & Eisner, L. (2023). Machine learning in microseismic monitoring. *Earth-Science Reviews*, 104371.
- Birnie, C., & Alkhalifah, T. (2022). Leveraging domain adaptation for efficient seismic denoising. In *Energy in data conference, austin, texas, 20–23 february 2022* (pp. 11–15).
- Birnie, C., & Hansteen, F. (2022). Bidirectional recurrent neural networks for seismic event detection. *Geophysics*, 87(3), KS97–KS111.
- Birnie, C., Jarraya, H., & Hansteen, F. (2021). An introduction to distributed training of deep neural networks for segmentation tasks with large seismic data sets. *Geophysics*, 86(6), KS151–KS160.
- Bose, S., Valero, H.-P., Liu, Q., Shenoy, R., & Ounadjela, A. (2009). An automatic procedure to detect microseismic events embedded in high noise. In *2009 seg annual meeting*.
- Carion, N., Massa, F., Synnaeve, G., Usunier, N., Kirillov, A., & Zagoruyko, S. (2020). End-to-end object detection with transformers. In *Computer vision—eccv 2020: 16th*

- europa conference, glasgow, uk, august 23–28, 2020, proceedings, part i 16 (pp. 213–229).
- Chen, Y. (2020). Automatic microseismic event picking via unsupervised machine learning. *Geophysical Journal International*, 222(3), 1750–1764.
- Dai, Z., Cai, B., Lin, Y., & Chen, J. (2021). Up-detr: Unsupervised pre-training for object detection with transformers. In *Proceedings of the ieee/cvf conference on computer vision and pattern recognition* (pp. 1601–1610).
- Eisner, L., Duncan, P. M., Heigl, W. M., & Keller, W. R. (2009). Uncertainties in passive seismic monitoring. *The Leading Edge*, 28(6), 648–655.
- Folesky, J., Kummerow, J., Shapiro, S. A., Häring, M., & Asanuma, H. (2016). Rupture directivity of fluid-induced microseismic events: Observations from an enhanced geothermal system. *Journal of Geophysical Research: Solid Earth*, 121(11), 8034–8047.
- Gibbons, S. J., & Ringdal, F. (2006). The detection of low magnitude seismic events using array-based waveform correlation. *Geophysical Journal International*, 165(1), 149–166.
- Grady, T. J., Khan, R., Louboutin, M., Yin, Z., Witte, P. A., Chandra, R., . . . Herrmann, F. J. (2022). *Model-parallel fourier neural operators as learned surrogates for large-scale parametric pdes* (Tech. Rep.). Technical Report TR-CSE-2022-1, 04 2022.
- Grubas, S., Yaskevich, S., & Duchkov, A. (2021). Localization of microseismic events using the physics-informed neural-network for traveltimes computation. In *82nd eage annual conference & exhibition* (Vol. 2021, pp. 1–5).
- Horne, S., Baird, A., Stork, A., & Naldrett, G. (2019). Machine learning for das microseismic event detection. In *81st eage conference and exhibition 2019 workshop programme* (Vol. 2019, pp. 1–5).
- Huang, & Alkhalifah, T. (2023). Microseismic source imaging using physics-informed neural networks with hard constraints. *arXiv preprint arXiv:2304.04315*.
- Huang, Li, J., Hao, H., & Li, X. (2018). Micro-seismic event detection and location in underground mines by using convolutional neural networks (cnn) and deep learning. *Tunnelling and Underground Space Technology*, 81, 265–276.
- Izzatullah, M., Yildirim, I. E., Waheed, U. B., & Alkhalifah, T. (2022). Laplace hypopinn: physics-informed neural network for hypocenter localization and its predictive uncertainty. *Machine Learning: Science and Technology*, 3(4), 045001.
- Kaven, J. O., Hickman, S. H., McGarr, A. F., & Ellsworth, W. L. (2015). Surface monitoring of microseismicity at the decatur, illinois, co2 sequestration demonstration site. *Seismological Research Letters*, 86(4), 1096–1101.
- Kumar, S., Vig, R., & Kapur, P. (2018). Development of earthquake event detection technique based on sta/lta algorithm for seismic alert system. *Journal of the Geological Society of India*, 92, 679–686.
- Larmat, C., Montagner, J.-P., Fink, M., Capdeville, Y., Tourin, A., & Clévéde, E. (2006). Time-reversal imaging of seismic sources and application to the great sumatra earthquake. *Geophysical Research Letters*, 33(19).
- Li, Zhang, H., Liu, S., Guo, J., Ni, L. M., & Zhang, L. (2022). Dn-detr: Accelerate detr training by introducing query denoising. In *Proceedings of the ieee/cvf conference on computer vision and pattern recognition* (pp. 13619–13627).
- Li, T., Gu, Y. J., Lawton, D. C., Gilbert, H., Macquet, M., Savard, G., . . . Yu, N. (2022). Monitoring co2 injection at the cami field research station using microseismic noise sources. *Journal of Geophysical Research: Solid Earth*, 127(12), e2022JB024719.
- Liu, Y., Wang, T., Zhang, X., & Sun, J. (2022). Petr: Position embedding transformation for multi-view 3d object detection. In *Computer vision—eccv 2022: 17th european conference, tel aviv, israel, october 23–27, 2022, proceedings, part xxvii* (pp. 531–548).
- Luo, Y., & Yang, F. (2014). Deep learning with noise. [hp://www.andrew.cmu.edu/user/fanyang1/deep-learning-with-noise.pdf](http://www.andrew.cmu.edu/user/fanyang1/deep-learning-with-noise.pdf).
- Maxwell, S. C., Rutledge, J., Jones, R., & Fehler, M. (2010). Petroleum reservoir characterization using downhole microseismic monitoring. *Geophysics*, 75(5), 75A129–75A137.

- McMechan, G. A. (1982). Determination of source parameters by wavefield extrapolation. *Geophysical Journal International*, *71*(3), 613–628.
- Mousavi, S. M., Ellsworth, W. L., Zhu, W., Chuang, L. Y., & Beroza, G. C. (2020). Earthquake transformer—an attentive deep-learning model for simultaneous earthquake detection and phase picking. *Nature communications*, *11*(1), 3952.
- Perol, T., Gharbi, M., & Denolle, M. (2018). Convolutional neural network for earthquake detection and location. *Science Advances*, *4*(2), e1700578.
- Rezatofighi, S. H., BG, V. K., Milan, A., Abbasnejad, E., Dick, A., & Reid, I. (2017). Deepsetnet: Predicting sets with deep neural networks. In *2017 IEEE International Conference on Computer Vision (ICCV)* (pp. 5257–5266).
- Shaheen, A., Waheed, U. b., Fehler, M., Sokol, L., & Hanafy, S. (2021). Groningenet: Deep learning for low-magnitude earthquake detection on a multi-level sensor network. *Sensors*, *21*(23), 8080.
- Shapiro, S., Dinske, C., & Rothert, E. (2006). Hydraulic-fracturing controlled dynamics of microseismic clouds. *Geophysical Research Letters*, *33*(14).
- Skoumal, R. J., Brudzinski, M. R., & Currie, B. S. (2016). An efficient repeating signal detector to investigate earthquake swarms. *Journal of Geophysical Research: Solid Earth*, *121*(8), 5880–5897.
- Song, C., Wu, Z., & Alkhalifah, T. (2019). Passive seismic event estimation using multi-scattering waveform inversion. *Geophysics*, *84*(3), KS59–KS69.
- Staněk, F., & Eisner, L. (2017). Seismicity induced by hydraulic fracturing in shales: A bedding plane slip model. *Journal of Geophysical Research: Solid Earth*, *122*(10), 7912–7926.
- Stork, A. L., Baird, A. F., Horne, S. A., Naldrett, G., Lapins, S., Kendall, J.-M., ... Williams, A. (2020). Application of machine learning to microseismic event detection in distributed acoustic sensing data. *Geophysics*, *85*(5), KS149–KS160.
- Sun, J., Xue, Z., Zhu, T., Fomel, S., & Nakata, N. (2016). Full-waveform inversion of passive seismic data for sources and velocities. In *2016 SEG International Exposition and Annual Meeting*.
- Vaezi, Y., & Van der Baan, M. (2015). Comparison of the sta/lta and power spectral density methods for microseismic event detection. *Geophysical Supplements to the Monthly Notices of the Royal Astronomical Society*, *203*(3), 1896–1908.
- Waldhauser, F., & Ellsworth, W. L. (2000). A double-difference earthquake location algorithm: Method and application to the northern Hayward fault, California. *Bulletin of the Seismological Society of America*, *90*(6), 1353–1368.
- Wamriew, D. S., Charara, M., & Maltsev, E. (2020). Deep neural network for real-time location and moment tensor inversion of borehole microseismic events induced by hydraulic fracturing. In *Spe Russian Petroleum Technology Conference*.
- Wang, & Alkhalifah, T. (2018). Microseismic imaging using a source function independent full waveform inversion method. *Geophysical Journal International*, *214*(1), 46–57.
- Wang, & Alkhalifah, T. (2021). Direct microseismic event location and characterization from passive seismic data using convolutional neural networks. *Geophysics*, *86*(6), KS109–KS121.
- Wang, Alkhalifah, T., bin Waheed, U., & Birnie, C. (2021). Data-driven microseismic event localization: An application to the Oklahoma Arkoma basin hydraulic fracturing data. *IEEE Transactions on Geoscience and Remote Sensing*, *60*, 1–12.
- Wang, T., Yuan, L., Chen, Y., Feng, J., & Yan, S. (2021). Pnp-detr: Towards efficient visual analysis with transformers. In *Proceedings of the IEEE/CVF International Conference on Computer Vision* (pp. 4661–4670).
- Warpinski, N. (2009). Microseismic monitoring: Inside and out. *Journal of Petroleum Technology*, *61*(11), 80–85.
- Wilkins, A. H., Strange, A., Duan, Y., & Luo, X. (2020). Identifying microseismic events in a mining scenario using a convolutional neural network. *Computers & Geosciences*, *137*, 104418.

- Ye, J., Gui, T., Luo, Y., Xu, Y., & Zhang, Q. (2021). One2set: Generating diverse keyphrases as a set. *arXiv preprint arXiv:2105.11134*.
- Young, R., & Maxwell, S. (1992). Seismic characterization of a highly stressed rock mass using tomographic imaging and induced seismicity. *Journal of Geophysical Research: Solid Earth*, *97*(B9), 12361–12373.
- Zhang, Luo, Z., Yu, Y., Cui, K., & Lu, S. (2022). Accelerating detr convergence via semantic-aligned matching. In *Proceedings of the ieee/cvf conference on computer vision and pattern recognition* (pp. 949–958).
- Zhang, H., Alkhalifah, T., Liu, Y., Birnie, C., & Di, X. (2022). Improving the generalization of deep neural networks in seismic resolution enhancement. *IEEE Geoscience and Remote Sensing Letters*, *20*, 1–5.
- Zheng, J., Lu, J., Peng, S., & Jiang, T. (2018). An automatic microseismic or acoustic emission arrival identification scheme with deep recurrent neural networks. *Geophysical Journal International*, *212*(2), 1389–1397.
- Zhu, X., Su, W., Lu, L., Li, B., Wang, X., & Dai, J. (2020). Deformable detr: Deformable transformers for end-to-end object detection. *arXiv preprint arXiv:2010.04159*.